Nanoscale Memory Characterization of Virus-Templated Semiconducting Quantum Dots

Nathaniel G. Portney,[†,⊥] Alfredo A. Martinez-Morales,[‡,⊥] and Mihrimah Ozkan[‡,§,*]

[†]Department of Bioengineering, [‡]Department of Electrical Engineering, and [§]Center for Nanoscale Science and Engineering, University of California, Riverside, California 92521. [⊥]These authors contributed equally to this work..

ABSTRACT We have developed a substrate-based bottom-up approach to assemble two different color emitting quantum dots (CdSe/ZnS core/shell QDs) on the surface of a novel virus mutant, CPMV-T184C. Electrical characteristics of individual hybrids were investigated by conductive atomic force microscopy for potential digital memory applications (*i.e.*, RAM). These individual 40 nm CPMV-QD(1,2) hybrids exhibited reversible bistable electrical behavior during repeatable writing—reading—erasing processes at the nanoscale.

KEYWORDS: CPMV · CdSe/ZnS quantum dots · nanoassembly · CAFM · nanoscale memory · nanoelectronics.

Viruses and inorganic nanocrystals are ideal nanoparticles that can be modified to exhibit surface properties amenable to nanoassembly for the development of nanoelectronics. Icosahedral viruses, such as cowpea mosaic virus (CPMV),[1,2] are packaged as a highly dense repeat of protein coat subunits within a convenient spherical nanoscale building block. CPMV is also compatible with some organic solvents (*e.g.*, dimethylformamide), pH and thermally stable,[1] and easily extracted and purified[2] serving as a flexible constituent for hybrid nanoassembly. With its known crystal structure[3] hybrid assemblies with CPMV have included conjugation with gold nanoparticles[4,5] and gold-coated substrates,[6] oligonucleotides,[7] and polymer systems.[8] Toward the nanoelectronics end, advanced organic electronic devices based on self-assembled redox molecules[9,10] or nanoparticle-incorporated polymers[11,12] have been demonstrated with repeatable conductance switching for memory applications. Previous quantum dot (QD) patterning with engineered bacteriophage,[13] characterization of CPMV with Au,[14] and tobacco mosaic virus for memory[15] show promise for bio-assisted patterning in nanoelectronics. Combining the novel multifunctional capability of viruses and optoelectronic QDs, we show CPMV-QD(1,2) as an exciting material system for electronic memory.

CPMV has a large number of aromatic residues (840 tryptophans per capsid[16]), and the insulating QD capping layer may provide a beneficial barrier for charge transfer. For example, stable electrical bistability with hysteresis was observed in spin-coated polyfluorene polymer with an Ag layer[17] and was suggested to be caused by charge transfer between polymer and an intermediate metal layer. Furthermore, nanogold particles with conjugated polyaniline fibers were proposed for memory by an electric field induced charge transfer effect, producing bistable switching as well.[18] Blum *et al.*[19] also showed an increase in conductivity of gold-nanoparticle-derivatized CPMV particles after conjugation with conductive molecules. By using a semiconductor instead of a metal, we chose to electrically characterize our CPMV-QD(1,2) hybrid system. Since current hybrid approaches in conjugated organic polymers have reported enhanced charge transfer by the addition of gold nanoparticles,[20] we were intrigued by the possibility of a similar effect between a highly aromatic CPMV system and the QDs.

We previously envisioned that solution-derived QD—CPMV[21] could be improved upon *via* a substrate approach, investigating biotemplated assembly of QDs and their electrical characterization for controlled assembly. Using a well-characterized, resilient, and labile CPMV-T184C template for QD addition, we have chosen to covalently couple two different color-emitting CdSe/ZnS core/shell QDs (QD_{red} and QD_{green}) on the viral capsid, visualizing particle addition by transmission electron microscopy (TEM), atomic force microscopy (AFM), and electrical characterization by conductive AFM (CAFM). CPMV-T184C mutant provides a

*Address correspondence to mihri@ee.ucr.edu.

Received for review April 27, 2007 and accepted December 19, 2007.

Published online January 10, 2008.
10.1021/nn700240z CCC: $40.75

uniform distribution of 60 surface cysteines and 300 lysines for multisite conjugation.

Using a substrate to initially anchor CPMV-T184C *via* a self-assembled monolayer (SAM) cross-linker on Au, followed by a stepwise approach to QD functionalization, aggregation issues are avoided, enabling multifunctional integration of our hybrid system. Initially, a SAM on Au deposition was performed using a 1:10 mixture of maleimide disulfide (MED) and hydroxyl-capped disulfide (EG3-EG3) in ethanol. The maleimide functional linker can attach to any protein containing a free cysteine with selective and efficient reactivity at pH ranges of 6.5–7.5.[22] Sulfhydryl ligands form metal complexes to gold with high binding affinity.[23] CPMV-T184C containing 60 cysteines per virion was then introduced to the SAM in the presence of 2 mM tris(carboxyethyl)phosphine (TCEP) reducing agent to produce a viral monolayer. Organic soluble red and green emitting ZnS capped CdSe QDs were hydrophilized by carboxylation and amination to facilitate aqueous based conjugation to the CPMV-T184C surface.[21,24] Green-emitting carboxylated QDs (QD_{green}-MAA) were covalently linked to the CPMV-T184C coat protein by activation with EDC (1-ethyl-3-(3-dimethylaminopropyl)carbodiimide hydrochloride) and subsequent attachment to lysine residues.[24,25] Amine-functionalized red-emitting QDs (QD_{red}-NH_3) were addressed with maleimide groups by reaction with the heterobifunctional cross-linker SMCC (succinimidyl 4-[*N*-maleimidomethyl]cyclohexane-1-carboxylate)[22,24] and then exposed to the remaining cysteines of the QD_{green}-modified CPMV-T184C particles.

TEM and energy dispersive X-ray spectroscopy (EDX) were used to characterize the viral surface morphologies and demonstrate QD decoration of monodispersed CPMV-T184C. The TEM grid was plasma oxidized (Harrick PDC-326 plasma cleaner) to adsorb hybrid lift-off solution before imaging at 100 kV (FEI-Philips CM300). Monodispersed CPMV-QD(1,2) hybrids were removed from the Au surface by incubation in water at 50 °C for 30 min, which is enough to disrupt the Au−S interactions without decomposing the virus particles.[1] The resulting solution was shown by absorbance spectrophotometry at 260 nm to contain 38 μg/mL of lifted off heterobifunctional CPMV-QD(1,2) particles, approximately 80% of total expected yield from the Au substrate (1 cm^2 Au area, 100nm $\langle d \rangle_{CPMV-CPMV}$ spacing, 5.6×10^6 g/mol). To spectroscopically verify that the dark regions on each virion of Figure 1A TEM were QDs, the EDX spectrum identified Cd, Se, Zn, and S elemental peaks consistent with ZnS capped CdSe cored QDs (Figure 1B). The sharp Cu peak is due to the Cu support of the TEM grid used for analysis. The strong Si peak comes from the Si wafer released from the hybrid lift-off procedure.

Atomic force microscopy in tapping mode was used to characterized the morphology (Figure 2A) of a monolayer of assembled CPMV-QD(1,2) hybrids on a gold-

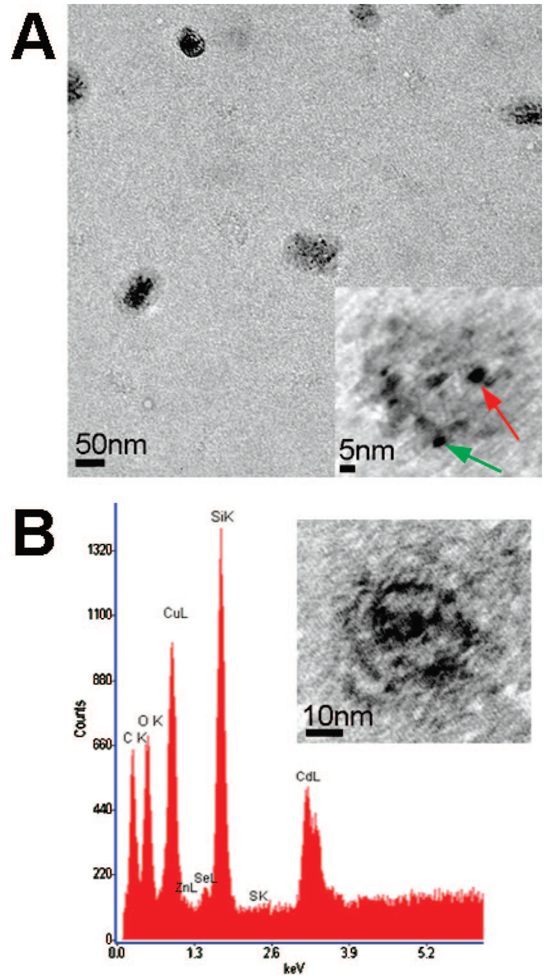

Figure 1. TEM and EDAX spectroscopy of CPMV-QD(1,2) hybrids on substrate and in solution. (A) TEM of unstained CPMV-QD(1,2) hybrid system thermally lifted off in solution at 24,000× and 100 kV, with a 50 nm scale bar. Micrograph shows well distributed monodispersed hybrids. High-resolution TEM in lower right at 205,000× and 100 kV (5 nm scale bar) shows presence of measured ~3.3 nm (green arrow) and ~6.1 nm (red arrow) QDs in black on a single 30 nm CPMV-T184C virus. Some particles appear less spherical due to possible denatured capsid or flattened viruses on the substrate, and hybrids appear larger than CPMV-T184C due to increased dimension by QD attachment. (B) Spectroscopy of representative CPMV-QD(1,2) hybrid by enhanced dispersive X-ray (EDAX) confirms local composition of QD by presence of Cd, Se, Zn, and S elements by the core and capping layer.

coated silicon (Au/Si) substrate. Textured regions throughout the monolayer indicate location of individual QDs on top of single virions. Inset in Figure 2A shows in greater detail the morphology of a single CPMV-QD(1,2) hybrid with dimensions of 40 nm in width and ~10 nm in height. Two different size QDs (QD_{red} and QD_{green}) can also be observed to be attached to its surface, and a cross section on the QD_{red} shows its dimensions to be ~7 nm (width) and 1 nm (height). Because a novel nanoparticle hybrid assembly involving the integration of two different size QDs on a single CPMV-T184C virus was developed, it was important to further analyze its morphology to clearly show the different nanomaterials integrating a single hy-

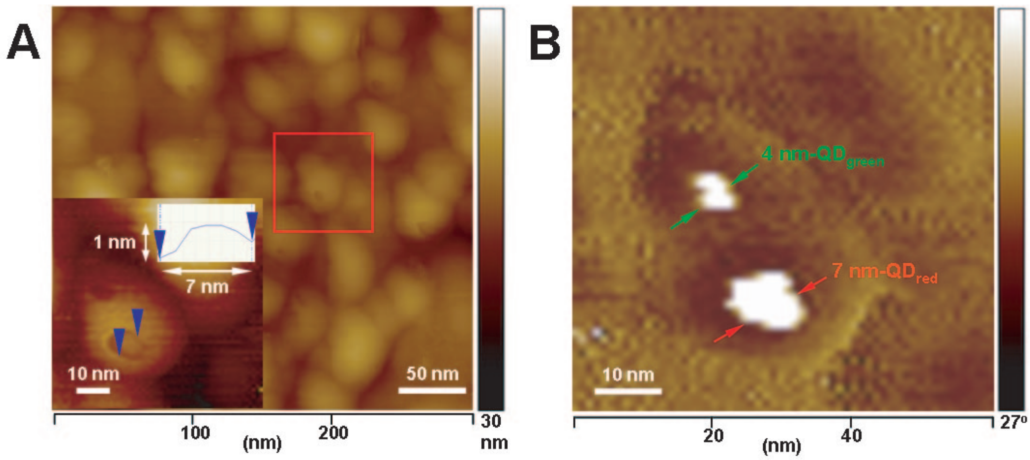

Figure 2. AFM characterization of CPMV-QD(1,2) hybrid. (A) Morphology AFM image in tapping mode of monolayer assembled nanoparticle hybrids. Inset shows in greater detail the morphology of a single CPMV-QD(1,2) hybrid and the cross section of a single QD_{red}. (B) phase AFM image of single CPMV-QD(1,2) hybrid clearly showing two different size QDs (QD_{red} and QD_{green}) attached to an individual virion.

brid. Figure 2B depicts the AFM image in phase mode of the hybrid shown in Figure 2A, inset. As observed, the QDs can be clearly differentiated from the virion due to the difference in the tip/sample interaction between the organic (virion) and inorganic (QDs) phase of the hybrid. The sizes of QDs (red and green) are in agreement with those obtained by TEM (7 and 4 nm, respectively).

All the electrical measurements on single hybrids were performed by CAFM in contact mode under an open air environment and ambient conditions. In a typical electrical characterization experiment, a "point and shoot" method was used to directly fix a conductive AFM tip (Pt/Ir coated Si tip with a radius of curvature <20 nm) on a single CPMV-QD(1,2) hybrid. All measurements were carried out by first taking a morphology scan of a monolayer of assembled CPMV-QD(1,2) hybrids and then driving the AFM tip to the top of a single hybrid where a measurement was directly taken across the CPMV-QD(1,2). For the purpose of the electrical characterization at the nanoscale, the Au/Si substrate was used as the bottom electrode while the stylus of the conductive tip was used as the top electrode with a single CPMV-QD(1,2) hybrid sandwiched in between both contacts as shown in Figure 3A (bottom). A total of 100 devices where tested, of which 81 showed bistability behavior. In order to demonstrate that the observed electrical bistability of the CPMV-QD(1,2) hybrid is due to the conjugation of a CPMV-T184C virion and QDs (red and green) rather than an electronic phenomenon caused by either one of the two nanomaterials composing the hybrid, we conducted electrical studies on CPMV-T184C and carboxylated QD_{green} as controls. Figure 3A (top) shows that conductance switching is absent in both control samples, supporting the conclusion that the conjugation between both nanomaterials (semiconducting QDs and insulating CPMV-T184C) is important for the observed memory effect.

Figure 3B shows the $I-V$ characteristics of a typical single CPMV-QD(1,2) hybrid. A memory effect can be observed when trace and retrace linear voltage scans are applied (−0.5 to 3.0 V and 3.0 to −0.5 V, respectively). As observed, the single hybrid is initially in a low conductivity state (defined as OFF state) until it reaches about 2.5 V where a sharp increase in conductivity occurs (defined as ON state), indicating the transition of the device from an initial OFF state to an ON state, equivalent to the "writing" process in a digital memory element. The hybrid remains at this high conductivity state as the voltage is continuously increased beyond 2.5 V. Out of 81 devices showing hysteresis, it was observed that seven devices retained a small current value at 0 V. The $I-V$ characteristics also show that the single hybrid can return to the initial OFF state by simply applying a reverse voltage bias—equivalent to the "erasing" process in a digital memory element. A third voltage scan from −0.5 to 3.0 V shows the hybrid's behavior to be nearly identical to the first voltage scan. This important feature could allow the application of CPMV-QD(1,2) hybrids to be used in a rewritable memory device. Furthermore, Figure 3B is a representative $I-V$ of 33 of the total 81 devices that showed a nanoscale memory effect during CAFM characterization. For these 33 devices, a turn-on voltage of 2.5 ± 0.5 V was measured.

Because two different size QDs were used, there are several possible scenarios for the tip/hybrid interaction during CAFM measurements on our CPMV-QD(1,2) hybrids, including (a) tip on red QD only, (b) tip on two interacting QDs (green and/or red), (c) tip on green QD only, and (d) tip on virus only without QD at all. The variations in these tip/sample configurations (a−c) affected the turn-on voltage observed in the $I-V$ curves. Using a zero-order approximation, the geometrical details of the interaction of the AFM tip with respect to the hybrid are ignored, and the AFM tip is ap-

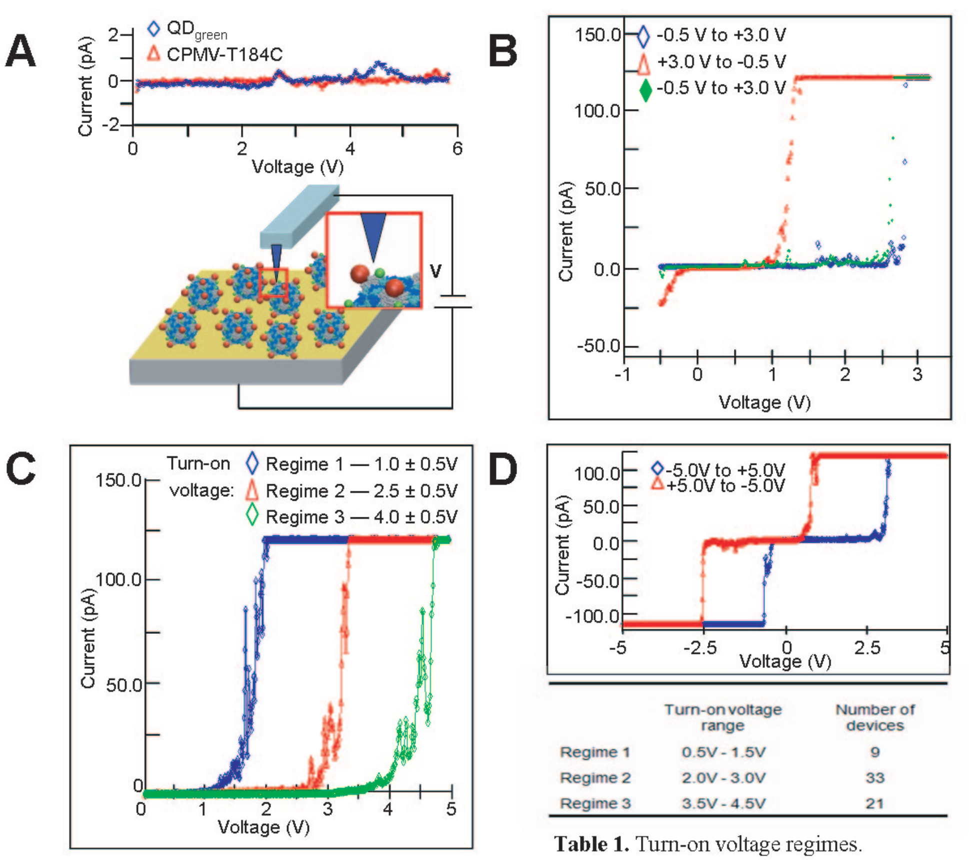

	Turn-on voltage range	Number of devices
Regime 1	0.5V - 1.5V	9
Regime 2	2.0V - 3.0V	33
Regime 3	3.5V - 4.5V	21

Table 1. Turn-on voltage regimes.

Figure 3. Electrical characterization by CAFM. (A) *I*−*V* curves for CPMV-T184C-only and QD$_{green}$ only configurations showing no switching behavior (top). Schematic of the setup used for the electrical characterization and implementation of a write-read-erase voltage cycle (bottom). (B) *I*−*V* characteristics of the CPMV-QD(1,2) hybrid demonstrating its electrical bistability behavior. When a voltage scan from −0.5 to 3.0 V is applied, conductance switching is observed on the CPMV-QD(1,2) hybrid. (C) *I*−*V* curve showing the three most predominant turn-on voltage regimes for the 100 CPMV-QD(1,2) hybrids tested. (D) *I*−*V* curve of a single CPMV-QD(1,2) hybrid under negative and positive bias. *I*−*V* shows a comparable electrical bistability under negative bias. Table 1 shows the number of devices that performed under the three main turn-on voltage regimes.

proximated as a sphere of ∼20 nm radius. Figure 3C shows superimposed the *I*−*V* curves for the three most predominant turn-on voltage regimes, which are believed to be caused by configurations (a−c). For configuration (d) the *I*−*V* can be observed in Figure 3A (top). Table 1 associated with Figure 3D shows the number of devices (out of 81) that fall into the three main turn-on voltage regimes. Figure 3D shows that hysteresis can also be observed under a negative bias.

In this hybrid system the QD CdSe core and the CPMV-T184C virus are separated by a high-gap ZnS semiconductor tunneling barrier. Here, the CPMV virus can behave as the charge donor during the conductivity switching allowing charge transfer to the lower-energy core. We suggest in this work, that an *E*-field induced charge transfer mechanism between the highly aromatic CPMV and the QD core is responsible for the observed electrical bistability of CPMV-QD(1,2) hybrids. Figure 4 shows a study on the conduction mechanism in both the ON and OFF states of the CPMV-QD(1,2) hybrid. The plot of log(*I*) as a function of $V^{1/2}$ (Figure 4A) could be fitted to a straight line, and from such linearity it can be observed that the conduction mechanism is probably due to thermionic emission.[26] Therefore, the conduction mechanism in the low conductivity state is dominated by charge injection from the electrode to the CPMV-T184C. Furthermore, a linear relation was also observe for the plot of log(*I*/*V*) as a function of $V^{1/2}$ in the high conductivity state, as shown in Figure 4B. From

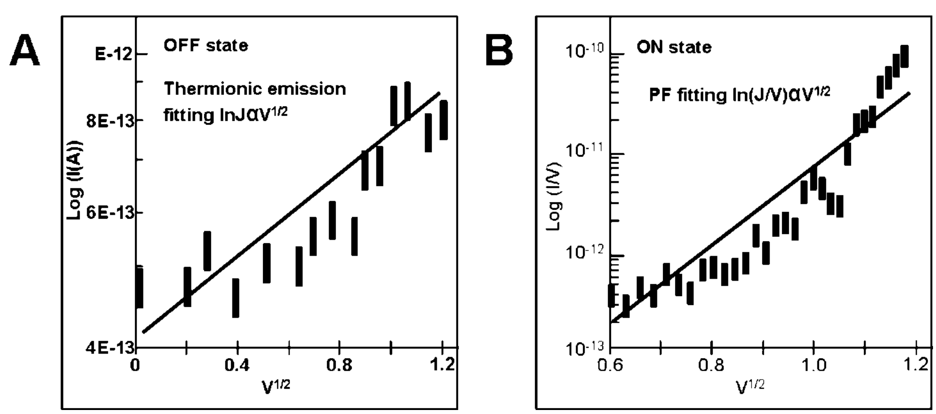

Figure 4. Analysis of the *I*−*V* characteristics for the CPMV-QD(1,2) hybrid during the low conductivity state (A) and the high conductivity state (B).

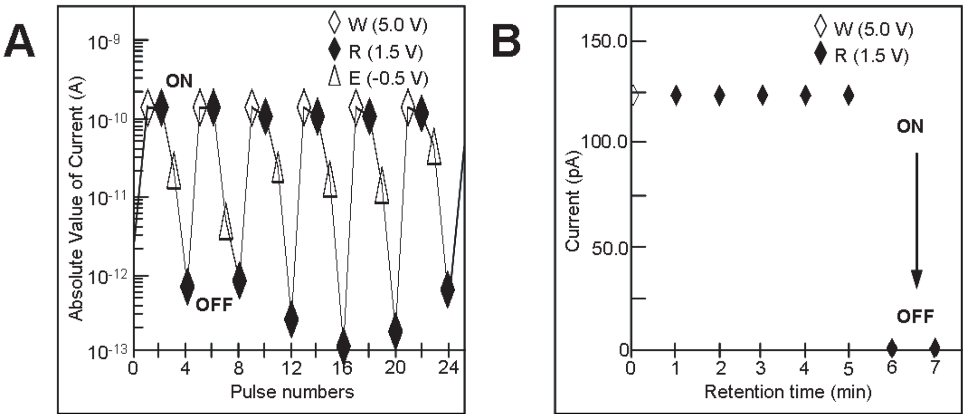

Figure 5. (A) *I*−*V* response of a single CPMV-QD(1,2) hybrid during write−read−erase voltage cycle (semilog plot). (B) Retention time of a single CPMV-QD(1,2) hybrid showing a single initial write and sequential reads at 1 min intervals.

this plot it can be observed that a Poole−Frenkel (PF)[27] emission is likely to be the conduction mechanism in the high conductivity state. Increasing to a higher potential helps overcome the high band gap ZnS cap potential barrier by tunneling and injects electrons into the CdSe core. When a threshold voltage is reached (*i.e.*, 2.5 V), the applied potential enables tunneling into the CdSe core, causing a high conductance switch. Hysteresis was observed in return scanning from high to low bias, suggestive of small charge storage in the QD core. In light of these results, we can hypothesize that the current conduction changed from an injection-dominated mechanism in low conductivity state to a charge-transport-dominated mechanism in the high conductivity state. In the case of the QD-only control the electric field induced by the applied potential is not enough to allow the charge carriers to tunnel through the QDs. It is, therefore, believed that the charge transfer process is the result of the charge donating ability of the CPMV's aromatic residues which enables the observed bistability behavior while it also provides a direct pathway to the charge transfer phenomenon. By analyzing the aromatic residue distribution (Figure S1), we can better understand how site attachment is taking place. At the same time the aromatic distribution shows a possible source for the charge transfer, where aromatic residues directly overlap with positions of QD attachment (yellow residues in asymmetric subunit), as shown in Figure S2.

On the basis of the experimental data acquired, a QD size dependence (*e.g.*, bandgap) is observed in the turn-on voltage. By use of a first-order approximation, these three regimes can be correlated to the number and/or size of the QD(s) across which the current is tunneling through. Therefore, considering that a higher bandgap would require a higher potential to induce tunneling across the CPMV-QD(1,2) hybrid, our results suggest that the three turn-on voltage regimes of 1.0 $\pm$ 0.5, 2.5 $\pm$ 0.5, and 4.0 $\pm$ 0.5 V correspond to the tip/sample configurations (a−c), respectively.

Furthermore, if the CPMV-QD(1,2) hybrid is to be used in future nanoelectronic devices (*i.e.*, ultradense memory), it is imperative to demonstrate that a single hybrid can function as an individual single memory element at the nanoscale. Figure 5A shows the *I*−*V* response of a single hybrid during a typical write−read−erase cycling process that was successfully carried for six complete cycles. During this cycling process, we probed the single hybrid with write, read, and erase voltage pulses of 5.0, 1.5, and −0.5 V, respectively. The corresponding currents to the different voltage pulses were recorded to clearly show the hybrid's switching behavior between two distinct conductance states (ON and OFF). A characteristic retention time of the ON state was obtained by measuring the conductivity state of the hybrid at 1 min intervals (Figure 5B) after an initial write pulse. The observed decay of the ON state during the charge retention measurements can be rationalized by two events that take place simultaneously during each measurement. First, because the CPMV-QD hybrid is partially composed of an organic material, the hybrid is inherently susceptible to local Joule heating effects. As such, some degradation of the CPVM-QD interface can be expected to take place each time a high potential is applied to the hybrid. At some point the CPMV-QD interface deteriorates to a point where the device fails to operate. A second plausible explanation deals with a thermionic drifting effect that is experienced by the AFM probe between subsequent electrical measurements. Although for most CAFM-based electrical measurements this probe drifting is negligible ($<$1 nm), in this work the effects can be quite significant due to the nanoscale nature of the measurements and the fact that probing of the CPMV-QD memory behavior is dictated by the interaction between the probe and hybrid.

As shown in Figures 3B−D and 5A,B, the high and low conductivity states are repeatable with high accuracy. Furthermore, this ability to write, read, and erase the conductivity state of the hybrid accomplishes the functionality of a memory device (*i.e.*, random access

ARTICLE

memory) and could expand the applicability of organic−QD hybrids into the realm of memory devices.

Although the nanoparticle toolset applied in this work can be considered rather exotic, the resilience and monodispersity of CPMV, combined with unique electronic properties of surface-passivated QDs, comprise a relevant material selection for hybrid nanoelectronic devices. Multisite patterning of two unique QDs was driven by a biotemplate on substrate approach (Figure S3), enhancing previous solution based bioconjugation. If the individual interconnect problems is addressed, based on observed electrical characterization, a single CPMV-QD(1,2) hybrid of 40 nm showing reversible bistable behavior shows promise for future digital memory applications.

Acknowledgment. We thank the FCRP and its focus center on Functional Engineered NanoArchitectronics (FENA) for the financial support. The authors thank G. Destito for his contribution in composing a model for the CPMV-QD(1,2) hybrid presented in this work. We also thank Dr. M.G. Finn and Dr. M. Manchester for providing CPMV viruses.

Supporting Information Available: Synthesis of QD-MAA, QD-AET, and QD-AET-SMCC nanoparticles, CPMV-T184C mutagenesis and isolation, preparation of MED/EG3-EG3 SAM and CPMV-T184C deposition, QD_{green} coupling efficiency to CPMV-T184C-QD(1,2), site selective QD immobilization on the CPMV-T184C virus particle and capsid organization, and space filling model of asymmetric subunit coat proteins of CPMV-T184C. This material is available free of charge *via* the Internet at http://pubs.acs.org.

REFERENCES AND NOTES

1. Virudachalam, R.; Harrington, M.; Markley, J. Thermal Stability of Cowpea Mosaic Virus Components: Differential Scanning Calorimetry Studies. *Virology* **1985**, *146*, 138–140.
2. Wang, Q.; Kaltgrad, E.; Lin, T.; Johnson, J. E.; Finn, M. G. Natural Supramolecular Building Blocks: Wild-Type Cowpea Mosaic Virus. *Chem. Biol.* **2002**, *9*, 805–811.
3. Lin, T.; Chen, Z.; Usha, R.; Stauffacher, C. V.; Dai, J.; Schmidt, T.; Johnson, J. E. The Refined Crystal Structure of Cowpea Mosaic Virus at 2.8 Å Resolution. *Virology* **1999**, *265*, 20–34.
4. Wang, Q.; Lin, T.; Johnson, J. E.; Finn, M. G. Natural Supramolecular Building Blocks: Cysteine-Added Mutants of Cowpea Mosaic Virus. *Chem. Biol.* **2002**, *9*, 813–819.
5. Wang, Q.; Lin, T.; Tang, L.; Johnson, J. E.; Finn, M. G. Icosahedral Virus Particles as Addressable Nanoscale Building Blocks. *Angew. Chem., Int. Ed.* **2002**, *41*, 459–462.
6. Cheung, C. L.; Camarero, J. A.; Woods, B. W.; Lin, T.; Johnson, J. E.; De Yoreo, J. J. Fabrication of Assembled Virus Nanostructures on Templates of Chemoselective Linkers Formed by Scanning Probe Nanolithography. *J. Am. Chem. Soc.* **2003**, *125*, 6848–6849.
7. Strable, E.; Johnson, J. E.; Finn, M. G. Natural Nanochemical Building Blocks: Icosahedral Virus Particles Organized by Attached Oligonucleotides. *Nano Lett.* **2004**, *4*, 1385–1389.
8. Raja, K. S.; Wang, Q.; Gonzalez, M. J.; Manchester, M.; Johnson, J. E.; Finn, M. G. Hybrid Vvirus-Polymer Materials. 1. Synthesis and Properties of PEG-Decorated Cowpea Mosaic Virus. *Biomacromolecules* **2003**, *4*, 472–476.
9. Collier, C. P.; Mattersteig, G.; Wong, E. W.; Luo, Y.; Beverly, K.; Sampaio, J.; Raymo, F. M.; Stoddart, J. F.; Heath, J. R. A [2]Catenane-Based Solid State Electronically reconfigurable Switch. *Science* **2000**, *289*, 1172–1175.
10. Cai, L.; Cabassi, M. A.; Yoon, H.; Cabarcos, O. M.; McGuiness, C. L.; Flatt, A. K.; Allara, D. L.; Tour, J. M.; Mayer, T. S. Reversible Bistable Switching in Nanoscale Thiol-Substituted Oligoaniline Molecular Junctions. *Nano Lett.* **2005**, *5*, 2365–2372.
11. Bozano, L. D.; Kean, B. W.; Beinhoff, B.; Carter, K. R.; Rice, P. M.; Scott, J. C. Organic Materials and Thin-Films Structures for Cross-Point Memory Cells Based on Trapping in Metallic Nanoparticles. *Adv. Funct. Mater.* **2005**, *15*, 1933–1939.
12. Ouyang, J.; Chu, C. W.; Szmanda, C. R.; Ma, L. P.; Yang, Y. Programmable Polymer Thin Film and Non-volatile Memory Device. *Nat. Mater.* **2004**, *3*, 918–922.
13. Lee, S.-W.; Mao, C.; Flynn, C. E.; Belcher, A. M. Ordering of Quantum Dots Using Genetically Engineered Viruses. *Science* **2002**, *296*, 892–895.
14. Blum, A. S.; Soto, C. M.; Wilson, C. D.; Cole, J. D.; Kim, M.; Gnade, B.; Chatterji, A.; Ochoa, W. F.; Lin, T.; Johnson, J. E.; Ratna, B. R. Cowpea Mosaic Virus as a Scaffold for 3-D Patterning of Gold Nanoparticles. *Nano Lett.* **2004**, *4*, 867–870.
15. Tseng, R. J.; Tsai, C.; Ma, L.; Ouyang, J.; Ozkan, C. S.; Yang, Y. Digital Memory Device Based on Tobacco Mosaic Virus Conjugated with Nanoparticles. *Nat. Nanotechnol.* **2006**, *1*, 72–77.
16. Poian, A.; Johnson, J. E.; Silva, J. L. Protein-RNA Interactions and Virus Stability as Probed by the Dynamics of Tryptophan Side Chains. *J. Biol. Chem.* **2002**, *277*, 47596–47602.
17. Ouisse, T.; Stephan, O. Electrical Bistability of Polyfluorene Devices. *Org. Electron.* **2004**, *5*, 251–256.
18. Tseng, R. J.; Huang, J.; Ouyang, J.; Kaner, R. B.; Yang, Y. Polyaniline Nanofiber/Gold Nanoparticle Nonvolatile Memory. *Nano Lett.* **2005**, *5*, 1077–1080.
19. Blum, A. S.; Soto, C. M.; Wilson, C. D.; Brower, T. L.; Pollack, S. K.; Schul, T. L.; Chatterji, A.; Lin, T.; Johnson, J. E.; Asminck, C.; Franzon, P.; Shashidhar, R.; Ratna, B. R. An Engineered Virus as a Scaffold for Three-Dimensional Self-Assembly on the Nanoscale. *Small* **2005**, *1*, 702–706.
20. Ouyang, J.; Chu, C.; Sieves, D.; Yang, Y. Electric-Field-Induced Charge Transfer Between Gold Nanoparticle and Capping 2-Naphthalenethiol and Organic Memory Cells. *Appl. Phys. Lett.* **2005**, *86*, 123507–123510.
21. Portney, N. G.; Singh, K.; Chaudhary, S.; Destito, G.; Schneemann, A.; Manchester, M.; Ozkan, M. Organic and Inorganic Nanoparticle Hybrids. *Langmuir* **2005**, *21*, 2098–2103.
22. HermansonG. T. *Bioconjugate Techniques*; Academic Press: San Diego, CA, 1996; p 148.
23. Bain, C. D.; Troughton, E. B.; Tao, Y.; Evall, J.; Whitesides, G. M.; Nuzzo, R. G. Formation of Monolayer Films by the Spontaneous Assembly of Organic Thiols from Solution onto Gold. *J. Am. Chem. Soc.* **1989**, *111*, 321–335.
24. Ravindran, S.; Chaudhary, S.; Colburn, B.; Ozkan, M.; Ozkan, C. S. Covalent Coupling of Quantum Dots to Multiwalled Carbon Nanotubes for Electronic Device Applications. *Nano Lett.* **2003**, *3*, 447–453.
25. Khorana, H. G. The Chemistry of Carbodiimides. *Chem. Rev.* **1953**, *53*, 145–166.
26. Rhoderick. E. H. Williams, R. H. *Metal-Semiconductor Contacts*; Clarendon: Oxford, 1988; pp80−87.
27. Choudhury, K. R.; Winiarz, J. G.; Samoc, M.; Prasad, P. N. Charge Carrier Mobility in an Organic-Inorganic Hybrid Nanocomposite. *Appl. Phys. Lett.* **2003**, *82*, 406–408.